A structural variant approach for establishing a detection limit in differential HX-MS measurements

Tyler S. Hageman[1] and David D. Weis[1,2,*]

[1]Department of Chemistry and the Ralph N. Adams Institute for Bioanalytical Chemistry,

[2]Department of Pharmaceutical Chemistry, University of Kansas

1567 Irving Hill Road, Lawrence, KS 66045

[*]Corresponding Author: dweis@ku.edu

ABSTRACT

Hydrogen exchange-mass spectrometry (HX-MS) is widely promoted for its ability to detect subtle perturbations in protein structure, but such perturbations will result in small differences in HX. However, the detection limit of HX-MS has not been widely investigated, nor is there a useful approach for defining the detection limit of HX-MS measurements. In this work, we designed a well-characterized structural variant spiking model to investigate the detection limit of conventional peptide-based HX-MS. The detection limit was challenged by spiking small fractions of a structural variant (modeled using maltose binding protein W169G mutant) into a reference protein (wild-type maltose binding protein). As little as 5% of the structural variant could be detected. The small structural perturbation was not resolvable by far UV circular dichroism, differential scanning calorimetry, or size exclusion chromatography. Furthermore, we validated the ability of the hybrid statistical analysis approach, presented in a companion paper (Hageman and Weis, Anal. Chem 2019), to reliably identify small, significant differences in HX-MS measurements. With our structural variant spiking model, we demonstrate a benchmarking approach for determining a detection limit of HX-MS for detection of changes in higher-order structure that might be encountered in protein structural comparability and similarity assessment applications.

INTRODUCTION

Detecting subtle changes in higher-order structures of proteins that relate to stability and function is an important analytical challenge. While X-ray crystallography and NMR are powerful methods capable of determining high-resolution protein structures and revealing changes in structure,[1-3] these methods can be limited by requirements such as crystallization, isotopic labeling, protein size, and low throughput. Alternative methods, such as circular dichroism (CD), differential scanning calorimetry (DSC), fluorescence, and infrared spectroscopy are routinely used for identifying changes in structure.[3,4] While these methods have higher throughput and generally consume less sample than X-ray crystallography and NMR, they lack resolution,

providing only global structural information. In contrast, hydrogen exchange-mass spectrometry (HX-MS) has proven to be useful for higher-order structural analysis, capable of providing localized structural information in a variety of applications.[5-8] To identify changes in structure, HX of two or more protein samples are compared to identify differences in HX kinetics.[9] Differences in HX can be localized in the protein primary structure by using bottom-up, middle-down, or top-down workflows.[10-14] In addition, identified HX differences can be mapped onto a solved or modeled three-dimensional protein structure to support the structural interpretation of HX-MS results.[15]

The magnitude of changes in higher-order structure will vary widely. Thus, the differences observed in differential HX-MS measurements could be large or small. For example, the observed HX differences in a high affinity protein-protein complex may be large, corresponding to the interaction interface.[16] In contrast, the observed HX differences as a result of a single residue modification may be small, corresponding to the impact of the modification.[17] When considering small differences in HX, a frequently asked question is “When is a difference real and significant?”. The continued growth in the use of HX-MS in the biopharmaceutical industry has emphasized addressing this question, especially for structural comparability of protein-based therapeutics during development and production and for biosimilars.[18,19] Traditionally, HX-MS is highlighted as a method that is capable of localizing subtle perturbations in higher-order structure. However, the detection limit of HX-MS for detecting subtle differences in protein structure has not been widely investigated.

A systematic investigation of detection limits in HX-MS has several requirements. First, a significance testing approach that reliably identifies significant differences in HX-MS measurements is essential because HX differences approaching the detection limit will be small. In our companion paper, we established a hybrid significance testing approach to reliably identify significant differences in HX-MS measurements. Next, a protein model in which the differences observed by HX can be related to the magnitude of change in structure is needed. An ideal model

would be a protein for which the higher-order structure could be systematically varied by a quantifiable amount. The differences in HX could then be correlated with the magnitude of change in structure. A model of this nature could be created by using denaturants to shift the conformational ensemble.[20] However with denaturants, maintaining the precision of the denaturant concentration would be a challenge. Instead of denaturants, point mutations could be used to slightly perturb structure. However, the change in structure from a mutation would need to be quantified and a wide panel of mutants would be necessary to challenge the HX-MS detection limit. Alternatively, the conformational ensemble of a reference protein could be artificially shifted by introducing fractions of a structural variant. Following this approach, the concentration of the structural variant could be varied to establish the detection limit of HX-MS. Thus, the detection limit of HX-MS could be defined by the lowest concentration of the structural variant when significant differences are observed in HX.

The goal when adding the structural variant is to slightly shift the observed HX relative to the amount of variant added. Ideally, the observed HX for each peptide will be a weighted average of HX by the structural variant and HX by the reference protein. This would only be the case for peptides from the structural variant and reference protein with the same sequence that co-elute. If the peptides or the retention times are different, then the observed HX will not be a weighted average but instead will be representative of only one of the two populations. Recently, Bonnington et al.[21] described HX-MS of an IgG1 monoclonal antibody (mAb) that was spiked with varying concentrations of a structural variant. In their study, the structural variant was generated by methionine oxidation. Following a bottom-up HX-MS workflow, increasing HX as a function of oxidized variant concentration was detected in peptides corresponding to the structurally perturbed regions. The peptides with oxidized methionines were not compared because the modified and unmodified peptides had different monoisotopic masses, different retention times, and likely different rates of back-exchange. Thus, in order to measure a limit of detection when using structural variant with primary structure modifications, it is essential that the structural

perturbations extend beyond the modification site. In the case of methionine oxidation of an IgG1 mAb, it is well documented that structural perturbations do extend beyond the oxidation site.[22,23] However, because there are multiple sites of modification, it is likely that there will be multiple subpopulations with differing amounts of oxidation and oxidation at different sites. Reproducibly generating a homogenously modified structural variant (e.g., singly oxidized at exactly one methionine) with chemical stress or even environmental stress is challenging. Heterogeneity in the structural variant will complicate HX-MS analysis because the sample will contain subpopulations with varying magnitudes of structural perturbation. For these reasons, a *homogenous* structural variant is more desirable. There are alternative modification approaches that are useful for generating homogenous structural variants of proteins such as N-terminal PEGylation, deglycosylation (i.e., for glycosylated proteins), or addition of a fusion protein.[18,24,25] To investigate the detection limit of HX-MS, we propose generating a structural variant having a single point mutation. The detection limit can then be determined by measuring the HX differences between the spiked and reference samples as a function of the amount of variant. In this way, homogeneity of the structural variant can be systematically controlled. A single point mutation will result in a different amino acid sequence at the mutation site. However, the mutation can be designed such that the structural perturbation extends beyond the mutation site. Furthermore, the designable aspect of point mutations offers the ability to vary structural perturbation by introducing conservative or aggressive mutations. In this work, we demonstrate the use of this structural variant model and hybrid significance testing approach (from our companion paper) as a general method to determine detection limits for HX-MS.

EXPERIMENTAL

Details of the expression and purification of wild-type (WT) maltose-binding protein (MBP) and mutant (W169G) MBP are described in the Supporting Information. Also described in the Supporting Information are the details about circular dichroism spectroscopy, differential scanning calorimetry, and size exclusion chromatography.

Hydrogen exchange-mass spectrometry (HX-MS)

MBP WT and W169G stock samples (50 μM) were removed from –80°C storage and adjusted to 8 μM with protein buffer. 5%, 10%, 15%, 20%, and 25% W169G spiked samples were prepared by volume-to-volume mixtures of WT and W169G at ratios of 19:1, 9:1, 17:3, 4:1, and 3:1, respectively. HX labeling was performed on a LEAP Technologies HDX PAL robot. Labeling was initiated by diluting 3 μL of 8 μM MBP samples in 57 μL of labeling buffer (100 mM sodium chloride, 20 mM sodium phosphate, pD 7.0 in D_2O, pH was corrected for isotope effect[26]). Each MBP sample was labeled at 25 °C in triplicate for each label time (30, 240, 1800, and 14400 s). After labeling, 50 μL of each sample was quenched with 50 μL of quench buffer (200 mM sodium phosphate, pH 2.5 in water) at 1 °C. All replicates for all samples of each individual HX labeling time were completed within a single day. Non-deuterated controls were identically prepared except with protein buffer (100 mM sodium chloride, 20 mM sodium phosphate, pH 7.0 in water) in the place of labeling buffer. Details of the HX-MS analysis are described in the companion paper.[Hageman and Weis, paper 1] 115 MBP peptic peptide assignments (94% sequence coverage, see **Figure S1** of the Supporting Information) were confirmed by CID-MS^2. With the peptic peptide database, HX-MS data files were processed in HDExaminer (versions 2.3 and 2.4, Sierra Analytics, Modesto, CA). After automated analysis, a single charge state that contained high quality spectra for all replicates, all samples, and across all HX labeling times was selected to represent HX for each peptide. The extent of HX based on peptide centroid mass (m) for each peptide at each HX label time was exported to Microsoft Excel and Systat SigmaPlot for post-processing. For each peptide at each HX label time, mean centroid masses ($\bar{m}$) were determined for triplicate measurements (n = 3). For HX uptake plots (Da vs. labeling time), the undeuterated centroid mass (m_0) for each peptide was subtracted from deuterated centroid masses. Within, we report differences in HX ($\Delta\overline{HX} = \bar{m}_{\mathrm{spike}} - \bar{m}_{\mathrm{WT}}$), where $\bar{m}_{\mathrm{spike}}$ is the mean centroid mass of a peptide for spiked samples and $\bar{m}_{\mathrm{WT}}$ is the corresponding peptide mean centroid mass for wild-

type MBP. All sample standard deviations (s_m) presented within this work were calculated using equation (1).

$$s_m = \sqrt{\frac{\sum_{i=1}^{n}(m_i - \bar{m})^2}{n-1}} \quad (1)$$

Hybrid significance testing was performed for all data following the approach demonstrated in our companion paper.[Hageman and Weis, paper 1] Additional details about the HX-MS experiments and calculations are provided in the Supporting Information.

RESULTS

In this work, we demonstrate an approach to establish a detection limit for differential HX-MS measurements. Furthermore, we demonstrate that the hybrid significance testing approach developed in our companion paper [Hageman and Weis, paper 1] can reliably identify subtle differences in higher-order structure that approach the detection limit. Maltose-binding protein (MBP) was selected as a model for this study because it is a well-characterized, stable, monomeric, and moderately sized protein (41.5 kDa). MBP wild-type (WT) and a mutant of MBP were used to model the reference protein and a structural variant, respectively. To generate a structural variant of MBP, a buried hydrophobic tryptophan (residue 169), residing in one of the two lobes of MBP, was substituted with a glycine. The MBP mutant structural variant (W169G) was spiked into WT to evaluate the detection limit for HX-MS. It is obvious that many analytical methods would be capable of detecting the spiked content of W169G solely based on the mutation itself (i.e., differences in *primary* structure); in this study the mutation was explicitly used to generate a *higher-order* structural variant.

The MBP mutant modestly altered higher-order structure

A structural variant model with subtle perturbation to structure is required in order to define the detection limit of HX-MS. Structural heterogeneity, such as a partially aggregated variant or heterogeneously oxidized methionines, will complicate analysis for determination of a detection limit. Meanwhile, a completely unfolded variant will not challenge the detection limit since there

would be gross differences in HX kinetics. Therefore, evaluating the integrity of the structural variant and characterizing the extent of perturbation to structure is essential. To evaluate the integrity of the structural variant and characterize the extent of perturbation induced by the mutation, samples of WT and W169G were compared by circular dichroism (CD), differential scanning calorimetry (DSC), size exclusion chromatography (SEC), and HX-MS. Overlaid far-UV CD spectra of WT and W169G indicate there are no major differences in overall secondary structure (see **Figure S2** of the Supporting Information). The W169G mutation decreased the thermal stability by 4°C based on far-UV CD and by 4.8°C based on DSC (see **Table S1** and **Figure S3** of the Supporting Information). SEC chromatograms (see **Figure S4** of the Supporting Information) show a 0.22 minute decrease in retention time for W169G suggesting that W169G has a larger hydrodynamic radius than WT (see **Table S1** of the Supporting Information). Overall, based on low-resolution biophysical techniques, the W169G mutation modestly destabilized the structure of MBP.

To evaluate impact of the W169G mutation on overall structure and conformational dynamics, intact HX-MS was measured for WT and W169G protein samples (intact HX-MS experiment details are provided in the caption of **Figure S5** of the Supporting Information). Intact HX of W169G was slightly faster than WT with a mean HX difference of +28 Da, equivalent to a +8% HX difference for 354 exchangeable backbone amides (see **Figure S5** of the Supporting Information). The increased backbone dynamics are consistent with the low-resolution biophysical measurements, indicating that the structure of MBP is modestly perturbed by the W169G mutation. To localize the extent of structural perturbation induced by the mutation,

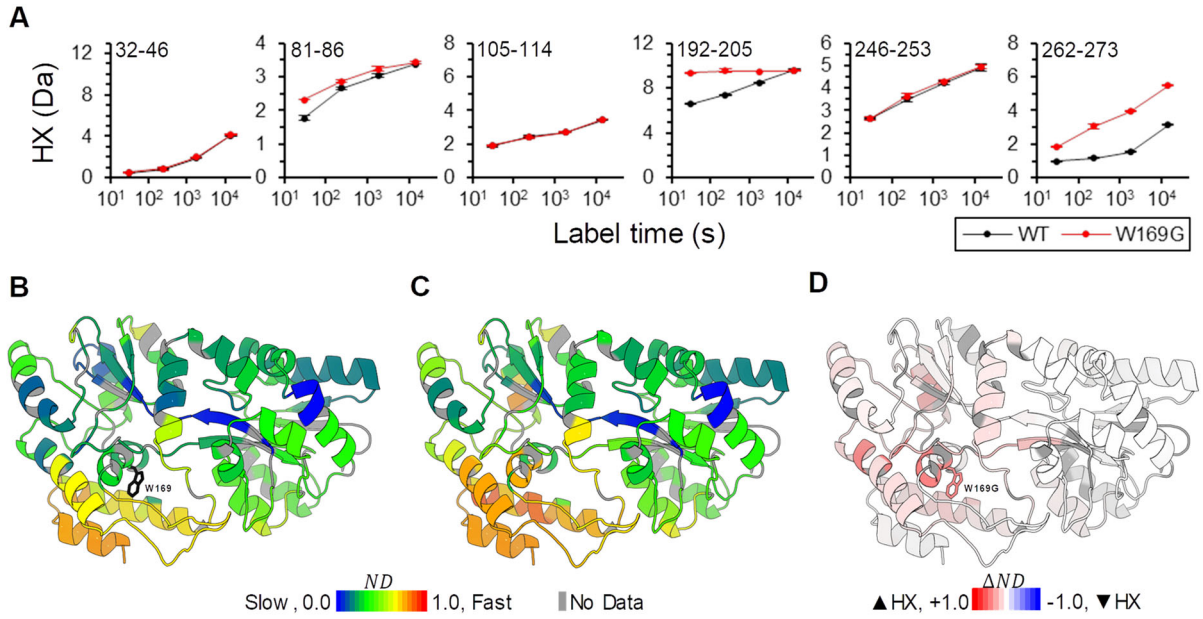

Figure 1. Representative peptide HX plots of WT (black) and W169G (red) (**A**); residue-averaged, normalized mean peptide HX (ND) values mapped onto a cartoon of a MBP 3-dimensional structure (PDB 1OMP[28]) for WT (**B**) and W169G (**C**); and the difference in ND values (**D**). For (**A**) the limits on the vertical axis are equal to the number of slowly back-exchanging amides for each peptide. For (**B**) and (**C**), the blue-red color gradient scale corresponds to ~~peptide~~resiude-~~resolved~~ averaged normalized deuteration ranging differences (ND) values[27] from 0.0 (no HX) to 1.0 (fast HX). W169 is denoted by black sticks in (**B**) and red sticks in (**D**). For (**D**), the red-white-blue color gradient scale corresponds to the peptide-resolved differences between W169G and WT normalized deuteration values, ΔND, where +1.0 is faster HX for W169G and –1.0 is slower HX for W169G. Regions colored grey represent residues for which HX values were not obtained because of missing coverage or by accounting for rapid back-exchange of the first two N-terminal residues of each peptide. Details of ΔND calculations are provided in the Supporting Information.

peptide-level HX-MS was performed. Representative HX plots comparing WT and W169G peptides are shown in **Figure 1A**. Peptides 32-46, 81-86, and 105-114 reside in the lobe not containing the mutation, while peptides 192-205, 246-253, and 262-273 reside in the lobe containing the mutation. Based on the structure of MBP,[28] peptides 81-86, 192-205, and 262-273, which show faster HX for W169G, are proximal to the mutation site, while peptides 32-46, 105-114, and 246-253, which show similar HX for W169G, are distal from the mutation site. To display the local impact of the mutation, residue-averaged, normalized mean peptide HX (ND) values[27,29] are mapped onto the structure of MBP for WT (**Figure 1B**) and W169G (**Figure 1C**). The

differences in normalized residue-averaged HX shows slightly faster HX for regions of W169G (**Figure 1D**). Regions with slightly faster HX are proximal to the lobe of MBP containing the W169G mutation. Residue-resolved HX obtained from peptide-level measurements shows W169G is locally destabilized, but many native structural features are conserved in the lobe of MBP without the mutation. Based on this extensive characterization, the W169G mutation modestly perturbed the higher-order structure which validates the suitability of this mutant as a structural variant to investigate the detection limit of HX-MS.

W169G mutant is a good model of a structural variant for HX-MS

To mimic a structural perturbation that slightly shifts the protein conformation ensemble for some regions while leaving other regions unaffected, we spiked MBP W169G, the structural variant, into WT MBP, the reference protein. Except for peptides containing the W169G mutation, the observed HX values for each peptide monitored in the spiked samples are thus expected to be a weighted average of HX by WT and HX by W169G. However, if the HX rates are very different, two separated isotopic spectral profiles would be observed or new peaks would appear on the higher m/z side of the spectral profile. This would suggest that the magnitude of structural perturbation of the structural variant is too large to define the detection limit. Also, a single centroid mass cannot be measured if there are two separated isotopic spectral profiles. Meanwhile, if the HX rates were only slightly different, the centroid mass of the isotopic spectral profile would shift slightly caused by increased abundance in the higher m/z peaks. Thus, the observed extent of HX would slightly increase, which is the desired outcome to define the detection limit. Based on the HX differences between the WT and W169G we expect to observe comparable HX rates for regions of MBP not impacted by the mutation (see **Figure 1D**) in all spiked samples. Meanwhile, the regions of MBP impacted by the mutation will shift the HX values in relation to the spiked fraction of the structural variant if the HX rates are only slightly different. However, if the HX rates are very different, then bimodal distributions will appear. Identifying subtle increases in HX resulting from slightly different HX rates will indicate the detection limit is being challenged.

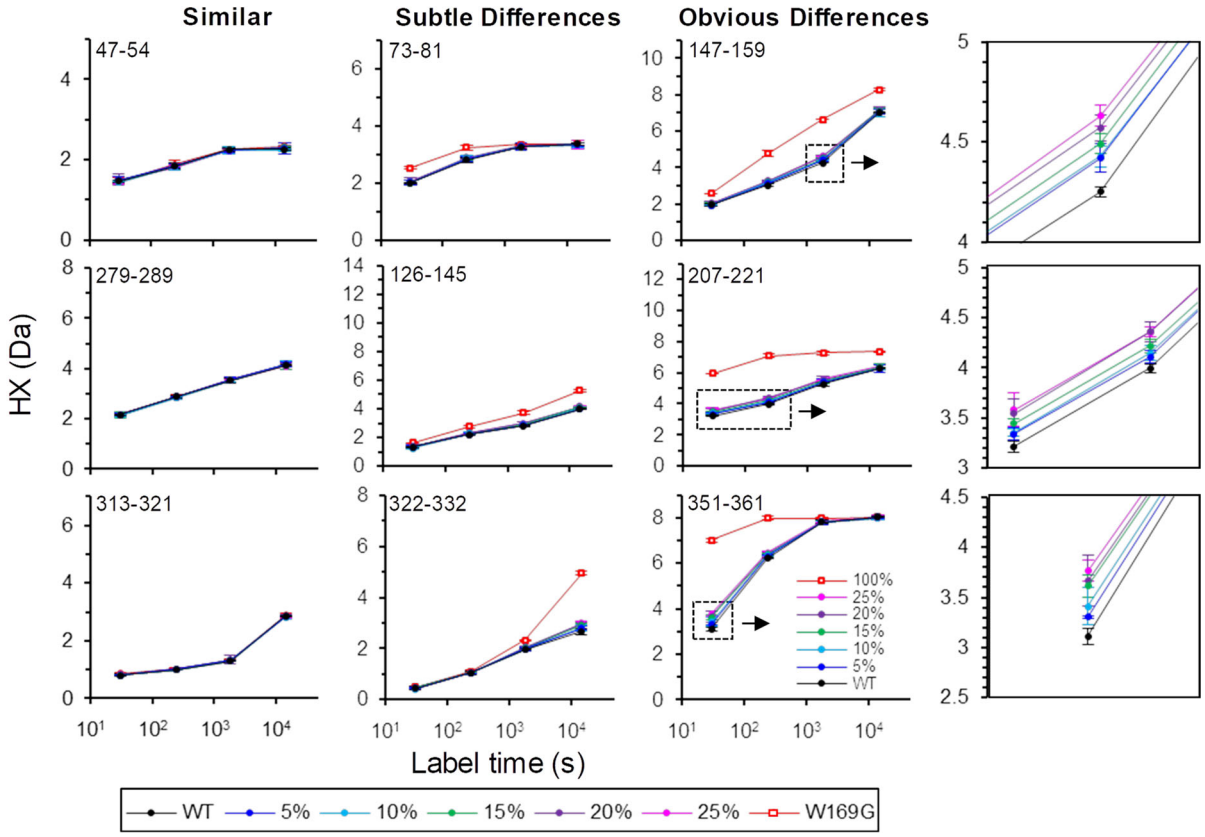

Figure 2. Representative peptide HX plots of WT (black); W169G (red); and spiked WT with W169G fractions of 5% (blue), 10% (cyan), 15% (green), 20% (purple) and 25% (pink). Error bars are 99% confidence intervals from triplicate measurements. Zoomed plots in the right-hand column correspond to the boxed regions (dashed black lines) with arrows in adjacent peptide HX plots. A complete set of HX plots for all peptides is available in **Figure S9** of the Supporting Information.

In the same manner as our WT and W169G HX-MS experiments, HX measurements were collected for samples with spiked W169G into WT at fractions ranging from 5% to 25%. HX in 115 peptic peptides, excluding peptides with the mutation site, were monitored (see coverage map in **Figure S1** of the Supporting Information). Peptides with the mutation site were excluded because the retention times are different and the observed HX is not a weighted average but instead is representative of each individual population.

Representative HX plots for 9 peptides are shown in **Figure 2**. HX was similar across all samples for peptides 47-54, 279-289, and 313-321, which are in the lobe of MBP without the mutation. HX by W169G was slightly faster for peptides 73-81 and 322-332, which also are in the

lobe of MBP without the mutation but are in the interface between the lobes and are proximal to the mutation site. Peptide 126-145, which resides in the mutation-containing lobe and is distal to the mutation site, shows slightly faster HX by W169G. HX by W169G is noticeably faster for peptides 147-159, 207-221, and 351-361, which span the mutation-containing lobe of MBP. Increased HX rates relative to fraction of structural variant is evident in the zoomed regions of the peptide HX plots where there are obvious HX differences between W169G and WT. As expected, the HX rate increases towards the HX rate of W169G as the fraction of structural variant increases.

A potential issue with an HX-MS spiking experiment of this nature is excessive structural perturbation in the structural variant. A large structural change (e.g., complete unfolding of the protein) will drastically increase the rate of HX by the structural variant. In this case, the HX-MS spectra for peptides in a structural variant spiked reference protein sample will contain separated isotopic spectral profiles (i.e., bimodal distributions) corresponding to the populations of reference protein and structural variant. A single centroid cannot be reliably used to determine the extent of HX for bimodal spectra.[30,31] None of the peptide mass spectra for W169G and WT protein samples show any completely separated isotopic spectral profiles (see **Figure S6** of the Supporting Information). One of the largest HX differences in our data was 3.9 Da for peptide 351-361 after 30 seconds of labeling. Even in this case, the isotopic spectral profiles overlap (see **Figure S6** of the Supporting Information). In the spiked samples, the distribution of peaks in isotopic spectral profiles shifted where differences were present between W169G and WT. In the case of the spiked samples, there were not any new peaks on the higher m/z side of the spectral profile. Rather, the abundance increased in the higher m/z peaks in the spectral profile (see **Figure S7** of the Supporting Information). Although there is a slight high mass skew in the isotopic distributions, the addition of the mutant does not cause severe distortions of the distributions. The absence of completely separated isotopic spectral profiles and the observation of differentially weighted isotopic spectral profiles with respect to fraction of structural variant spiked in our data,

demonstrates that our structural variant spiking model is suitable to investigate a detection limit for HX-MS.

Establishing a detection limit for HX-MS

Faster HX by the spiked samples is evident in the peptide HX plots in **Figure 2**. However, subjective interpretation of the HX plots for 115 peptides is not suitable to evaluate significance of differences in HX, nor for establishing a detection limit. An objective significance test is needed to detect significant differences in order to establish a detection limit because the magnitude of significant HX differences will be small. In our companion paper [Hageman and Weis, paper 1] we validated a hybrid significance testing approach that reliably identifies significant differences in large differential HX-MS data sets using null measurements of WT MBP. In hybrid significance testing, significance is determined by evaluating the observed difference in HX ($\Delta\overline{HX}$) against a defined global $\Delta\overline{HX}$ significance threshold representative of experimental error. Any observed $\Delta\overline{HX}$ exceeding the global threshold is filtered by a second significance criterion, Welch's *t*-test, that evaluates the observed $\Delta\overline{HX}$ in relation to technical replicate variability. The hybrid significance testing results can be displayed using a volcano plot, with $\Delta\overline{HX}$ on the horizontal axis, *p*-value on the vertical axis, and marked significance limits results that exceed significance criteria. To evaluate the capability of this approach to reveal subtle differences in differential HX-MS data, we applied it to our HX-MS structural variant spiking data.

Our spiking data had a pooled standard deviation of 0.030 Da, the same value we found in our previous null experiments of MBP WT presented in our companion paper. Using the pooled standard deviation, a global $\Delta\overline{HX}$ significance threshold was determined to be ±0.110 Da (see Supporting Information). The results of hybrid significance testing are displayed as volcano plots in **Figure 3A**. The $\Delta\overline{HX}$ significance limits (vertical red dashed lines) at +0.110 Da and –0.110 Da represent the calculated global significance threshold, while the *t*-test significance limits (horizontal red dashed lines) represent α = 0.01 for Welch's *t*-test. Any data point exceeding both

limits is classified as significant. In the volcano plots, significant differences are obvious in the spiked samples and the number of significant differences increases with the fraction of spiked structural variant, as quantified in **Figure 3B**. The absence of significant differences in 0% spiked

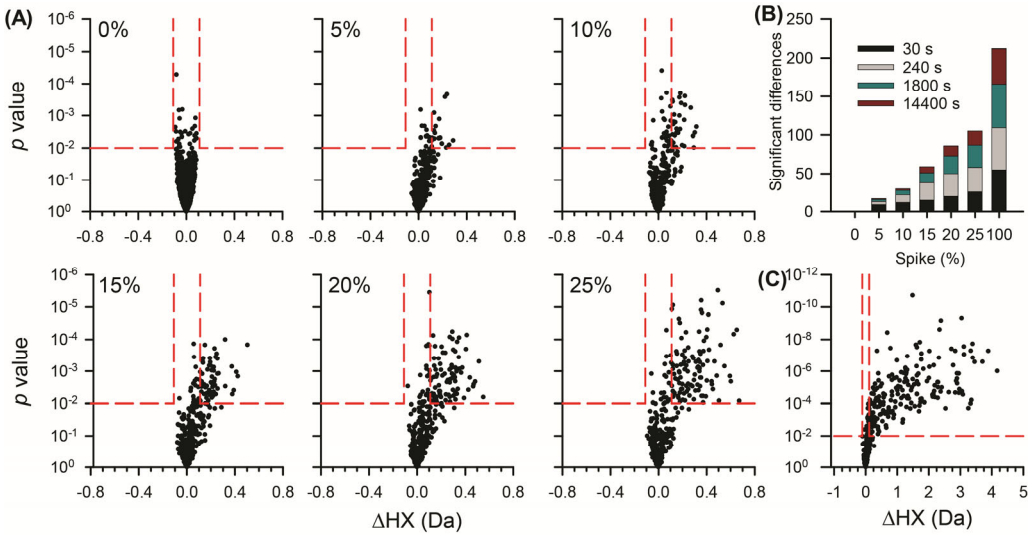

Figure 3. Volcano plots of observed $\Delta\overline{HX}$ values (horizontal axis) and Welch's *t*-test *p*-values (vertical axis) for 0% (null comparisons of MBP WT), 5%, 10%, 15%, 20%, and 25% MBP W169G spiked samples (**A**). Number of significant differences identified from hybrid significance testing (**B**). No significant differences were found in the 0% spiked sample (i.e., null comparisons of MBP WT). 5. Volcano plot for W169G (i.e., 100%) and WT (i.e., 0%) comparison (**C**). This figure uses different axis scales. For the volcano plots, the horizontal *p*-value significance limits (red dashed lines) are defined at α = 0.01 and vertical significance limits (red dashed lines) are defined at ±0.110 Da from s_p calculated $\Delta\overline{HX}$ significance limits representative of α = 0.01, as detailed in the Supporting Information.

samples (i.e., no false positives) validates the reliability of the differences classified as significant in the spiked samples. These results indicate the detection limit of HX-MS with this MBP model is less than 5% of the structural variant. A positive bias (ΔHX > 0 Da) in the distribution of data in the 5% sample compared to null is also notable suggesting that altered HX in the *collection* of measurements might be detectable even if individual differences are not significant.

To confirm the reliability of the differences classified as significant in the spiked samples, we compared significant differences in spiked samples to significant differences identified in the W169G sample (i.e., 100% spiked). A volcano plot of hybrid significance testing results for HX differences between W169G and WT is shown in **Figure 3C**. Supporting Information **Figure S8**

summarizes all significant results compared with 100% spiked sample. The much larger number of significant differences identified in the 100% spiked sample than in the 5-25% spiked samples in **Figure 3**, shows there are many false negatives in the 5-25% spiked samples. These false negatives indicate there are many HX differences in the 5-25% spiked samples that simply fall below the HX detection limit. Conversely, any significant difference identified in a spiked sample that is not also identified in the 100% spiked sample must be a type I error (i.e., false positive). No such false positives were observed.

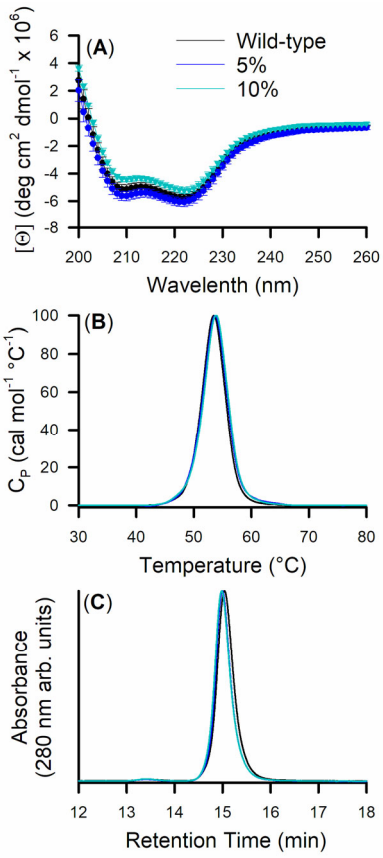

Figure 4. Far-UV CD spectra (**A**), DSC thermograms (**B**), and SEC chromatograms (**C**) of WT, 5% spiked, and 10% spiked samples.

Spiking challenges the detection limit of conventional biophysical techniques

DSC and SEC detected differences between WT and W169G (see **Figures S3** and **S4** of the Supporting Information). To compare the HX-MS detection limit with detection limits for the

biophysical methods, samples containing 5% and 10% spiked structural variant were compared to WT by CD, DSC, and SEC as shown in **Figure 4**. The 5% and 10% spiked MBP samples were essentially indistinguishable from the wild-type sample. The intensity of absorbance in the mean CD spectrum of the 10% spiked samples is slightly different (**Figure 4A**). Given the differences observed in the baseline at 260 nm for the 10% spiked samples, the mean CD spectrum for 5% and 10% spiked structural variant samples are similar within the repeatability of the measurement. The thermograms from DSC were also indistinguishable (see **Figure 4B**) and there is no evidence of a shoulder at a lower thermal transition temperature which would indicate detection of W169G in 5% and 10% spiked samples. The thermal transition temperatures obtained from CD melts and DSC were equal within experimental error (see **Table S1** of the Supporting Information). SEC chromatograms of 5% and 10% spiked samples (**Figure 4C**) are similar to WT and there is no evidence of chromatographic peak shoulders at earlier retention times indicating the presence of W169G. Although the biophysical techniques were capable of distinguishing WT and W169G, these methods did not resolve distinguishable differences between the 5% and 10% spiked samples and the WT. Meanwhile, with HX-MS, differences were readily identified in 5% and 10% spiked samples.

DISCUSSION

In this study, our objective was to demonstrate a structural variant spiking approach that can be used to establish a detection limit for HX-MS. We generated a structural variant by introducing a mutation that modestly perturbed the higher-order structure of MBP. Then we spiked the structural variant into the reference protein at different fractions, performed HX-MS measurements, and using differential HX, compared the extent of HX between spiked and reference samples. Because there were only modest differences in the structural variant, the differences in HX in the spiked samples were subtle. In order to determine a detection limit, a reliable statistical analysis approach was necessary to determine significance for these differences. In our companion paper, we demonstrated that a hybrid significance testing approach

is superior, in terms of type I and type II error, to commonly used approaches. Here in this work, to evaluate the ability of the hybrid significance testing approach to identify subtle changes in higher-order structure, we applied hybrid significance testing to our spiking results. The resulting volcano plots, displaying hybrid significance testing criteria, show an increase in the number of significant differences as the fraction of spiked structural variant increases. In **Figure 5**, the regions exhibiting significantly different HX are mapped onto the structure of MBP. The significant differences correspond to peptides in the vicinity of the mutation. The progressive expansion of the significant differences as the fraction of structural variant increases is consistent with the impact of the W169G mutation shown in **Figure 1D**. These results demonstrate that the hybrid significance testing approach is reliable for identifying subtle changes in higher-order structure using differential HX-MS measurements.

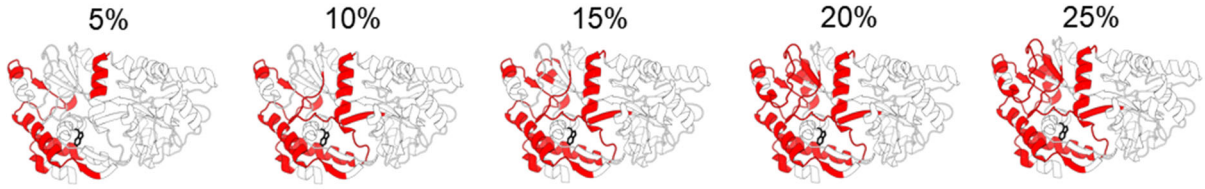

Figure 5. Peptides classified as significant (red) by hybrid significance testing (**Figure 3**) mapped onto a cartoon of the structure for MBP (PDB 1OMP). The tryptophan side chain displayed as black sticks corresponds to the site of the mutation (W169G).

Significant differences were detected using HX-MS in samples with as little as 5% structural variant, indicating that the detection limit for this particular structural variant is less than 5%. Estimating an absolute HX-MS detection limit is challenging because the number of significant differences is not a linear function of spiked fraction of structural variant. In this study, the ~5% detection limit is representative only for this particular structural variant. The degree of structural perturbation in the variant is a critical component of the detection limit. The detection limit will depend on the structural perturbation in the variant. A larger fraction (i.e., higher detection limit) of a variant with minor structural perturbation may be necessary to observe significant

differences in HX. In contrast, a ~~smaller fraction (i.e., lower detection limit)~~ might be found for ~~of~~ a variant with major structural perturbation. For example, Bonnington et al. estimated a detection limit of 1% for a mAb variant generated by methionine oxidation.[21] There is an unmet need for a deeper understanding of the interplay between HX kinetics and protein structural changes. For this purpose, structural variant spiking HX-MS experiments with a structurally well-defined and characterized variant would be invaluable.

The design of the structural variant is a critical factor. Here we used a single point mutation. Other approaches such as induced oxidation and altered glycosylation have proven useful to generate a structural variant for spiking studies.[21,32] However, unlike these other approaches, the mutation approach offers more control of sample homogeneity because the variant is itself homogeneous. Also, a mutation approach is not constrained to specific residues and locations since a mutation can be designed for nearly any residue in a protein. Regardless of the approach used to generate a structural variant, the structural changes should be irreversible (i.e., not refolding in dilute buffer conditions), free of heterogeneity, and should induce subtle changes that will approach the detection limit. A potential limitation of a structural variant spiking approach to investigate the detection limit of HX-MS arises from relying on a minority population to shift the measured HX signal (i.e., centroid of the isotopic spectral profile) of the major population. A large structural perturbation in the minority population might result in complete separation of HX signals of the major and minor populations. To avoid this limitation, one could compare HX-MS by directly comparing a mutant with one or more conservative mutations to wild-type. The challenge in such an approach would be quantifying the structural changes between the populations to determine the detection limit. With a spiking approach, the detection limit can be defined simply by the fraction spiked. Meanwhile, the degree of structural perturbation in the structural variant is related to the detection limit. Thus, identifying the degree of structural perturbation by extensive characterization of the structural variant is important to provide credibility in the determined detection limit.

To date there has not been a study to determine the detection limit of HX-MS using a homogenous, well-defined spiked-in structural variant. Our results with such a model demonstrate that HX-MS is capable of detecting a structural variant that was below the limit of detection of conventional biophysical methods. In a similar context, comparability and similarity assessments of higher-order structure of protein-based therapeutics has placed greater demands on traditional characterization methods to detect subtle structural changes that could potentially impact product quality. In particular, the growing market of biosimilars highlights the need for methods that can demonstrate structural similarity in support of licensing. Although this need cannot be met by any single method, improved methods to substantiate similarity of higher-order structure are desirable. HX-MS is a popular candidate for fulfilling this role. Thus, determination of detection limits of HX-MS for structural changes is essential. Our study demonstrates a benchmarking approach for determining a detection limit of HX-MS for detecting subtly altered structure that might be encountered in ~~structural~~ comparability assessment applications. The relatively low detection limit of HX-MS for structural changes, compared to other conventional biophysical approaches, suggests that HX-MS could be sufficiently sensitive to subtle changes in structure that it would ~~a~~ be useful ~~method~~ for establishing similarity of higher-order structure for therapeutic proteins. However, to evaluate similarity, alternative statistical approaches are necessary: significance should be demonstrated in terms of equivalence testing rather than in terms of the absence of significant differences.

ACKNOLEDGEMENTS

We thank Agilent Technologies for an instrument loan, Jeff Morrow for HDExaminer software support, the Macromolecule and Vaccine Stabilization Center at University of Kansas for assistance with biophysical characterization, the National Institutes of Health NIGMS Biotechnology Predoctoral Training Program (T32-GM008359) and the National Science Foundation (CHE-1709176) for financial support.

REFERENCES

(1) Kendrew, J. C.; Bodo, G.; Dintzis, H. M.; Parrish, R. G.; Wyckoff, H.; Phillips, D. C. *Nature* **1958**, *181*, 662. DOI: 10.1038/181662a0.
(2) Kaptein, R.; Boelens, R.; Scheek, R. M.; Van Gunsteren, W. F. *Biochemistry* **1988**, *27*, 5389-5395. DOI: 10.1021/bi00415a001.
(3) Cooper, A. *Biophysical chemistry*, 2nd ed.; The Royal Society of Chemistry: Cambridge, UK, 2011.
(4) Vedadi, M.; Arrowsmith, C. H.; Allali-Hassani, A.; Senisterra, G.; Wasney, G. A. *Journal of structural biology* **2010**, *172*, 107-119. DOI: 10.1016/j.jsb.2010.05.005.
(5) Smith, D. L.; Deng, Y.; Zhang, Z. *Journal of Mass Spectrometry* **1997**, *32*, 135-146.
(6) Houde, D.; Arndt, J.; Domeier, W.; Berkowitz, S.; Engen, J. R. *Anal Chem* **2009**, *81*, 2644-2651. DOI: 10.1021/ac802575y.
(7) Marciano, D. P.; Dharmarajan, V.; Griffin, P. R. *Current opinion in structural biology* **2014**, *28*, 105-111. DOI: 10.1016/j.sbi.2014.08.007.
(8) Pirrone, G. F.; Iacob, R. E.; Engen, J. R. *Analytical chemistry* **2015**, *87*, 99-118. DOI: 10.1021/ac5040242.
(9) Wales, T. E.; Engen, J. R. *Mass Spectrometry Reviews* **2005**, *25*, 158-170. DOI: 10.1002/mas.20064.
(10) Leurs, U.; Mistarz, U. H.; Rand, K. D. *Eur J Pharm Biopharm* **2015**, *93*, 95-109. DOI: 10.1016/j.ejpb.2015.03.012.
(11) Pan, J.; Zhang, S.; Borchers, C. H. *Biochim Biophys Acta* **2016**, *1864*, 1801-1808. DOI: 10.1016/j.bbapap.2016.08.013.
(12) Brown, K. A.; Wilson, D. J. *Analyst* **2017**, *142*, 2874-2886. DOI: 10.1039/C7AN00662D.
(13) Karch, K. R.; Coradin, M.; Zandarashvili, L.; Kan, Z.-Y.; Gerace, M.; Englander, S. W.; Black, B. E.; Garcia, B. A. *Structure* **2018**, *26*, 1651-1663.e1653. DOI: https://doi.org/10.1016/j.str.2018.08.006.
(14) Brodie, N. I.; Huguet, R.; Zhang, T.; Viner, R.; Zabrouskov, V.; Pan, J.; Petrotchenko, E. V.; Borchers, C. H. *Analytical Chemistry* **2018**, *90*, 3079-3082. DOI: 10.1021/acs.analchem.7b03655.
(15) Zhang, A.; Hu, P.; MacGregor, P.; Xue, Y.; Fan, H.; Suchecki, P.; Olszewski, L.; Liu, A. *Anal Chem* **2014**, *86*, 3468-3475. DOI: 10.1021/ac404130a.
(16) Malito, E.; Faleri, A.; Lo Surdo, P.; Veggi, D.; Maruggi, G.; Grassi, E.; Cartocci, E.; Bertoldi, I.; Genovese, A.; Santini, L.; Romagnoli, G.; Borgogni, E.; Brier, S.; Lo Passo, C.; Domina, M.; Castellino, F.; Felici, F.; van der Veen, S.; Johnson, S.; Lea, S. M., et al. *Proceedings of the National Academy of Sciences, USA* **2013**, *110*, 3304-3309. DOI: 10.1073/pnas.1222845110.
(17) Yan, Y.; Wei, H.; Fu, Y.; Jusuf, S.; Zeng, M.; Ludwig, R.; Krystek, S. R., Jr.; Chen, G.; Tao, L.; Das, T. K. *Anal Chem* **2016**, *88*, 2041-2050. DOI: 10.1021/acs.analchem.5b02800.
(18) Houde, D.; Berkowitz, S. A.; Engen, J. R. *J Pharm Sci* **2011**, *100*, 2071-2086. DOI: 10.1002/jps.22432.
(19) Wei, H.; Mo, J.; Tao, L.; Russell, R. J.; Tymiak, A. A.; Chen, G.; Iacob, R. E.; Engen, J. R. *Drug Discov Today* **2014**, *19*, 95-102. DOI: 10.1016/j.drudis.2013.07.019.
(20) Walters, J.; Milam, S. L.; Clark, A. C. *Methods in enzymology* **2009**, *455*, 1-39. DOI: 10.1016/S0076-6879(08)04201-8.
(21) Bonnington, L.; Lindner, I.; Gilles, U.; Kailich, T.; Reusch, D.; Bulau, P. *Anal Chem* **2017**, *89*, 8233-8237. DOI: 10.1021/acs.analchem.7b01670.
(22) Liu, D.; Ren, D.; Huang, H.; Dankberg, J.; Rosenfeld, R.; Cocco, M. J.; Li, L.; Brems, D. N.; Remmele, R. L., Jr. *Biochemistry* **2008**, *47*, 5088-5100. DOI: 10.1021/bi702238b.

(23) Torosantucci, R.; Schoneich, C.; Jiskoot, W. *Pharm Res* **2014**, *31*, 541-553. DOI: 10.1007/s11095-013-1199-9.
(24) Houde, D.; Berkowitz, S. A. *J Pharm Sci* **2012**, *101*, 1688-1700. DOI: 10.1002/jps.23064.
(25) Arbogast, L. W.; Brinson, R. G.; Formolo, T.; Hoopes, J. T.; Marino, J. P. *Pharm Res* **2016**, *33*, 462-475. DOI: 10.1007/s11095-015-1802-3.
(26) Glasoe, P. K.; Long, F. A. *The Journal of Physical Chemistry* **1960**, *64*, 188-190. DOI: 10.1021/j100830a521.
(27) Keppel, T. R.; Weis, D. D. *Journal of The American Society for Mass Spectrometry* **2015**, *26*, 547-554. DOI: 10.1007/s13361-014-1033-6.
(28) Sharff, A. J.; Rodseth, L. E.; Spurlino, J. C.; Quiocho, F. A. *Biochemistry* **1992**, *31*, 10657-10663. DOI: 10.1021/bi00159a003.
(29) Xia, Y.; Diprimio, N.; Keppel, T. R.; Vo, B.; Fraser, K.; Battaile, K. P.; Egan, C.; Bystroff, C.; Lovell, S.; Weis, D. D.; Anderson, J. C.; Karanicolas, J. *Journal of the American Chemical Society* **2013**, *135*, 18840-18849. DOI: 10.1021/ja407644b.
(30) Guttman, M.; Weis, D. D.; Engen, J. R.; Lee, K. K. *J Am Soc Mass Spectrom* **2013**, *24*, 1906-1912. DOI: 10.1007/s13361-013-0727-5

10.1007/s13361-013-0727-5. Epub 2013 Sep 10.
(31) Sarpe, V.; Schriemer, D. C. In *Hydrogen exchange mass spectrometry: Theory, techniques, and applications*, Weis, D. D., Ed.; Wiley, 2016, pp 37-54.
(32) Arbogast, L. W.; Delaglio, F.; Schiel, J. E.; Marino, J. P. *Anal Chem* **2017**, *89*, 11839-11845. DOI: 10.1021/acs.analchem.7b03571.

TOC FIGURE